Nonlinear three-dimensional Rayleigh-Taylor instability

S. I. Abarzhi*

Department of Mathematics, University of North Carolina at Chapel Hill,† Chapel Hill, North Carolina 27599

The Rayleigh-Taylor instability is studied for an incompressible inviscid fluid of infinite depth for three-dimensional (3D) spatially periodic flow. The problem is formulated in terms of general conditions that allow one to find the symmetry of the observable steady structures. Analytical steady solutions for a hexagonal type of flow symmetry (plane group $p6mm$) are found in few orders of approximations. Interrelations between the results with various types of flow symmetry are established. Comparisons with previously studied 3D flows with ''square'' and ''rectangular'' symmetries are given.
[S1063-651X(98)14312-X]

PACS number(s): 47.20.−k, 52.35.Py

I. INTRODUCTION

The Rayleigh-Taylor instability (RTI) is the instability of a heavy fluid layer (water) supported by a light fluid layer (air) in a uniform gravity field [1]. RTI is a general phenomenon in physics with a wide range of applications in astrophysics, lasers, plasmas, turbulence, fusion, etc. [2]. Often experiments are performed in a region where fluids are deep and differ greatly in densities. Surface tension and viscosity regularize the fluid motion and establish the most unstable mode [3]. For small Weber and large Reynolds numbers, the Rayleigh-Taylor instability has a short-wave character, and experiments show the following stages in the instability development. Small perturbations of the fluid-free surface quickly increase with increment $\tau^{-1} \sim \sqrt{g/\lambda}$, where g is the uniform acceleration and λ is the perturbation wavelength [2]. Rather fast, at perturbation amplitude $\sim 0.1\lambda$, the periodic bubbles-jet structure forms: water is carried down in the jets and air is coming up in the bubbles. At time $t \gg \tau$, the velocity of rising bubbles becomes constant and the motion is steady. At later times, new coherent structures appear, and the typical flow scale grows. Eventually, turbulent mixing breaks the ordered fluid motion [2,4,5].

At the present time, there is not a complete theoretical description of the Rayleigh-Taylor instability. The first theoretical RTI studies have been performed by Taylor [4], Layzer [6], Garabedian [7], and Birkhoff [8]. The theories agree reasonably with experimental results but could not explain all observable RTI features. In 1957, Garabedian was the first to put forward a hypothesis that the steady solution is not unique [7]. For a 2D flow, the quantitative verification of Garabedian's hypothesis has been obtained in [9]. It is well known that as a rule the Rayleigh-Taylor instability is a spatial process because the periodic ''plane'' fluid motion is unstable and eventually becomes three-dimensional [2]. The 3D flow is extremely complex, but some progress for spatial RTI has been reached in recent research [10–13].

Under some experimental conditions, [2,4,5], the Rayleigh-Taylor instability is a short-wave instability, the modes are coupling weakly, and, at a finite time, an order imposed by the initial perturbation is preserved, while the final turbulent RTI stage is a complete disorder. These features of RTI allow one to apply the symmetry theory to the problem. In this work, we consider the spatial Rayleigh-Taylor instability on the basis of the general symmetry analysis.

II. SYMMETRY ANALYSIS FOR THE RAYLEIGH-TAYLOR INSTABILITY

Let us consider the motion of inviscid incompressible fluid with the potential $\Phi(\mathbf{r},z,t), \mathbf{r}=(x,y)$. The experimental situation is well reflected in this theoretical approximation at linear and nonlinear stages of the instability [2,4,5]. At any time t the flow is described by the Laplace equation with the boundary conditions at infinity and at the free fluid surface $z - z^*(\mathbf{r},t) = 0$:

$$\Delta\Phi = 0, \quad \nabla\Phi|_{z=+\infty} = 0,$$

$$\left.\frac{\partial\Phi}{\partial t}\right|_{z=z^*} + \tfrac{1}{2}(\nabla\Phi)^2 + gz|_{z=z^*} = 0, \quad \frac{\partial z^*}{\partial t} + \nabla z \nabla\Phi|_{z=z^*} = 0. \tag{1}$$

Asymptotically, at $t \gg \tau$, the motion becomes steady: $\partial\Phi/\partial t = 0$ and $\partial z^*/\partial t = 0$ [2,4,5].

In formulation (1), the typical scale of the instability is defined by initial perturbation. For better agreement with RT experiments, the wavelength of the initial perturbation can be chosen in the vicinity of the most unstable mode [3–5]. Dependence on initial data is one of the most interesting questions in the Rayleigh-Taylor instability. It is an experimental fact that the late time asymptotes of incompressible RTI are essentially independent of initial data for small-amplitude initial perturbations, but a dependence occurs in a certain case [2]. It should be noted that apart from ''traditional''

*Present address: University of Bayreuth, Institute for Theoretical Physics, Bayreuth 95440, Germany. FAX: +49-921-555820. Electronic address: snezha@uni-bayreuth.de

†FAX: +1-919-962-5228. Electronic address: snezha@math.unc.edu
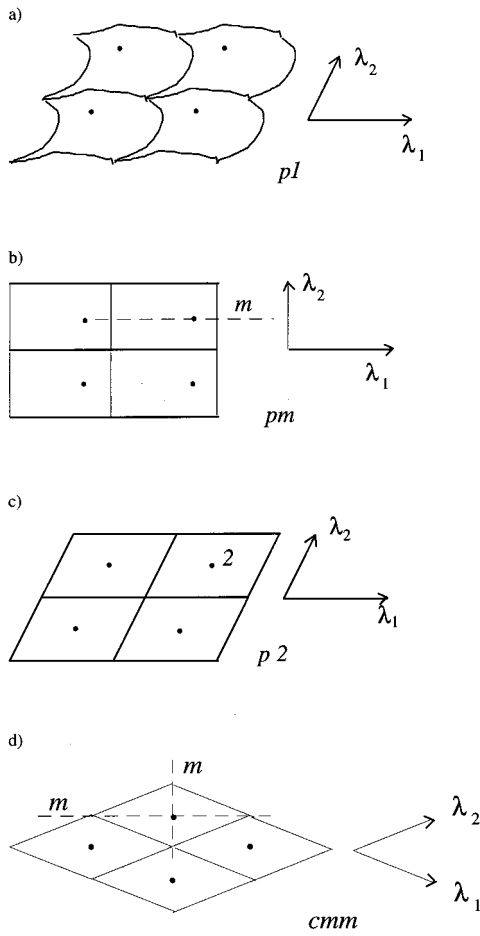
FIG. 1. Symmetry groups of the flow. The plane (x,y) of the flow (fluid-free surface or velocity field). Groups $p1$, pm, $p2$, cmm, and λ_i, spatial periods, rotation axis 2, and mirror planes m are perpendicular to the plane of translations. Black circles mark the positions of maximum point (bubble top). Motions are unstable (a),(b) and stable (c),(d) with respect to spatial noise $\mathbf{q}$ in the plane (x,y).

amplitude dependence, in three-dimensional RTI a new problem will have to be posed. Namely, what is to be the symmetry of the initial perturbation to generate the steady flow in RTI?

Let us assume that the initial perturbation at $t=0$ is spatially periodic: $\Phi(\mathbf{r}+n_1\boldsymbol{\lambda}_1+n_2\boldsymbol{\lambda}_2,z^*,0)=\Phi(\mathbf{r},z^*,0)$ and $z^*(\mathbf{r}+n_1\boldsymbol{\lambda}_1+n_2\boldsymbol{\lambda}_2,0)=z^*(\mathbf{r},0)$, where $\boldsymbol{\lambda}_1,\boldsymbol{\lambda}_2$ are the vectors of translations in the plane (x,y). Since the problem is periodic, there is the physical equivalence of points and directions, and the flow (1) is invariant with respect to a symmetry group. Vortices or traveling waves with an oscillatory time dependence $\sim e^{iwt}$ have never been observed in RTI, so this symmetry group is one of 17 space groups G including a subgroup of translations in a plane (here, we use international classification [14] for these 17 "two-dimensional" crystallographic groups. For example, the notation $pgm2$ describes the group with the following symmetry elements: periodicity in the x and y directions (small p), twofold axis along the z axis (number 2), and two planes of reflections, mirror (m) and glide (g), along the z axis) [14] Fig. 1.

We consider the flow (1) as a smooth one. Thus, in the

plane (x,y) of initial perturbation there are no gaps or overlaps, and a small-amplitude initial perturbation is taken to be analytical. To observe experimentally a periodic structure of bubble-jets, some conditions of stability must be satisfied. Actually, at least at finite time, the observed structure is stable with respect to spatial noise, and its macroscopic dynamics is prescribed by a main spatial mode: bubbles are neither merging nor splitting. These natural conditions can be easily reformulated in the language of symmetry theory.

Let us classify the initial perturbation in terms of irreducible representations of wave vectors $\{\mathbf{k}^*\}$ in G [14,15]. These wave vectors determine the flow translation invariance in time. At $t\ll\tau$, the flow symmetry is defined by that wave vector $\mathbf{K}^*$, subgroup $G_{\mathbf{K}*}$, associated with the strongest growth (greatest increment).

If modes related to various wave vectors $\{\omega_{\mathbf{k}*}\}$ are coupled weakly (do not intersect), the irreducible representations of the wave vectors are not mixing, and macroscopic dynamics of the system is determined by $\mathbf{K}^*$ [15]. This assumption of weakly coupled modes is usable as soon as there is no change of the spatial periodicity of the flow, and the solution (1) is smooth and analytical over the free surface. Note that the symmetry analysis requires a hierarchy of the modes but does not restrict the number of higher-order Fourier harmonics of initial perturbation. Experiments and numerical research [4,5,10,11,16,17] confirm this assumption of the immiscible modes. In fact, it is the reason for the accurate agreement between Layzer's theory and experimental data [4,5,6]. Evidently, the finite (large) amplitude of initial perturbation, surface tension, and viscosity will play a crucial role for the mode mixing [3,10,18].

Although weak coupling of the modes is an important condition, taken alone, it is insufficient to generate a stable periodic structure in RTI. Actually, assume that modes $\{\omega_{\mathbf{k}*}\}$ interact weakly and the wave vector $\mathbf{K}^*$ defines macroscopic dynamics of the system. Then, the subgroup $G_{\mathbf{K}*}$ of this wave vector determines the stability of the structure $\mathbf{K}^*$ with respect to noise [14,15]. To explain this statement, let us consider a macroscopically modulated structure with spatial period $\mathbf{K}^*+\mathbf{q}$, $\mathbf{q}=(q_x,q_y)$, where $q\lambda\ll1$. Let us make the expansion of the solution (or fluid thermodynamic potential) in terms of small $\mathbf{q}$. For the structure $\mathbf{K}^*$ to be stable with respect to noise, this expansion must be extreme at $\mathbf{q}=\mathbf{0}$ with no terms linear in components of $\mathbf{q}$: $\Phi(\mathbf{K}^*+\mathbf{q})-\Phi(\mathbf{K}^*)\sim Fq^2$, $F>0$. To provide this form of the expansion, vectors $\mathbf{q}$ and $-\mathbf{q}$ are needed to be equivalent with respect to symmetry operations, $G_{\mathbf{K}*}(\mathbf{q})=G_{\mathbf{K}*}(-\mathbf{q})$ [15]. In this way, the following conclusion can be drawing. If there are no special reasons to form a quasiperiodic structure the subgroup $G_{\mathbf{K}*}$ of the stable periodic structure $\mathbf{K}^*$ should contain the inversion $G_{\mathbf{K}*}(\mathbf{k})=G_{\mathbf{K}*}(-\mathbf{k})$, Fig. 1.

Another important stability condition is the conservation of rotation symmetry elements at given translations $\mathbf{K}^*$. This condition is necessary to form a sole bubble in the unit cell with the instability development. Among 17 groups G, the symmorphic groups allow the occurrence of only the maximum point (or bubble) in the unit cell. For nonsymmorphic groups (for example, $p4mg$, pmg, and $pgg2$), no point in the unit cell is immovable with respect to the symmetry operations [14], and the maximum point (bubble) is bound not to be unique.

The above conditions, in fact, provide the stability of the periodic structure with respect to disruptions of its macroscopic homogeneity. It should be noted that analogous requirements are in common use for order-disorder transitions [15].

Let G be the invariance group of the flow (1) at $t=0$ and this initial perturbation be of small amplitude. Assume that with the instability development up to $t \gg \tau$, the flow is smooth, the irreducible representations of wave vectors $\{\mathbf{k}^*\}$ in G are not mixing, the structure related to the wave vector $\mathbf{K}^*$ is stable, and at given translations the number of rotation symmetry elements is unchanged. As we have seen, these symmetry requirements provide the explanation for the experimental observation of the spatially periodic structure of bubble jets in the RT instability.

Each of the 17 space groups can be considered on the basis of the above symmetry analysis. As evidenced by the above, a periodic steady flow can be generated by RTI for that initial perturbation invariant with respect to a symmorphic group posing inversion (central point). Groups $p6mm$, $p4mm$, $pmm2$, and cmm are some of them, Fig. 1. For groups with no inversion, such as $p1$, pm, pg, and pmg, any structures (including the ''strongest growth'' structures) are unstable with respect to spatial modulations, and for these groups the observation of the steady motion fails, Fig. 1.

For illustration, let us consider the small-amplitude initial perturbation invariant with respect to the hexagonal spatial symmorphic group $G=p6mm$ [14] in Eqs. (1). This group allows the occurrence of a sole bubble (maximum point) in the unit cell, Fig. 2. If $\boldsymbol{\lambda}_1, \boldsymbol{\lambda}_2$ are the translations in the plane $|\boldsymbol{\lambda}_1|=|\boldsymbol{\lambda}_2|=\boldsymbol{\lambda}$, $\boldsymbol{\lambda}_2=G(\boldsymbol{\lambda}_1)$, with angle $\boldsymbol{\lambda}_1\boldsymbol{\lambda}_2=2\pi/3$, the unit vectors of inverse lattice $\mathbf{k}_i$ are defined by the relation $\mathbf{k}_i\boldsymbol{\lambda}_j=2\pi\delta_{ij}$, $ij=1,2$, Fig. 2.

That wave vector $\mathbf{k}^*$ with general position in the inverse space has the subgroup of identity transformation $G_{\mathbf{k}*}=1$. The wave vector $\mathbf{k}^*=0$ subgroup is the pointed group $G_{\mathbf{k}*}=6mm$. This wave vector corresponds to periods $\{\boldsymbol{\lambda}_1, \boldsymbol{\lambda}_2\}$ in real space. The other wave vectors are $\mathbf{k}^*=\mathbf{k}_1/2$, $G_{\mathbf{k}*}=2mm$, vectors of translations $\{2\boldsymbol{\lambda}_1, \boldsymbol{\lambda}_2\}$; $\mathbf{k}^*=(\mathbf{k}_1+\mathbf{k}_2)/3$, $G_{\mathbf{k}*}=3m$, vectors of translations $\{3\boldsymbol{\lambda}_1, 3\boldsymbol{\lambda}_2\}$; $\mathbf{k}^*=\mu\mathbf{k}_1$, $G_{\mathbf{k}*}=m$; $\mathbf{k}^*=\mu(\mathbf{k}_1+\mathbf{k}_2)$, $G_{\mathbf{k}*}=m$, vectors of translations $\{\boldsymbol{\lambda}_1/\mu, \boldsymbol{\lambda}_2\}$ and $\{\boldsymbol{\lambda}_1/\mu, \boldsymbol{\lambda}_2/\mu\}$, respectively, with $\mu>1/2$ [14,15].

Evidently, the wave vector $\mathbf{k}^*=\mathbf{0}$ corresponds to unchanged spatial periods and to the shortest of all possible translations. At $t\ll\tau$, the strongest growth of the instability relates to $\mathbf{K}^*=\mathbf{0}$. As long as spatial modes $\{\omega_{\mathbf{k}*}\}$ interact weakly, this wave vector describes the macroscopic dynamics of the system. Its subgroup $G_{\mathbf{k}*}=6mm$ contains inversion, so the periodic structure of the bubbles is stable with respect to spatial modulations, at least at finite time. Hence, one would expect that at $t\gg\tau$, the steady flow will have symmetry $p6mm$ and spatial period $\boldsymbol{\lambda}$, Fig. 2.

Similarly, it is easily shown that for each of the symmorphic groups, $p4mm$, $pmm2$, $p2$, and cmm (3D spatial flow) or group $pm11$ in the degenerate case of 2D flow, the symmetry and periods of the initial perturbation can be preserved up to the steady motion stage [5,9,12,13].

As has been found in [13], in the limiting case of tensionless fluid (1), there is a family of steady solutions and the dimension of this multitude is defined by the symmetry of
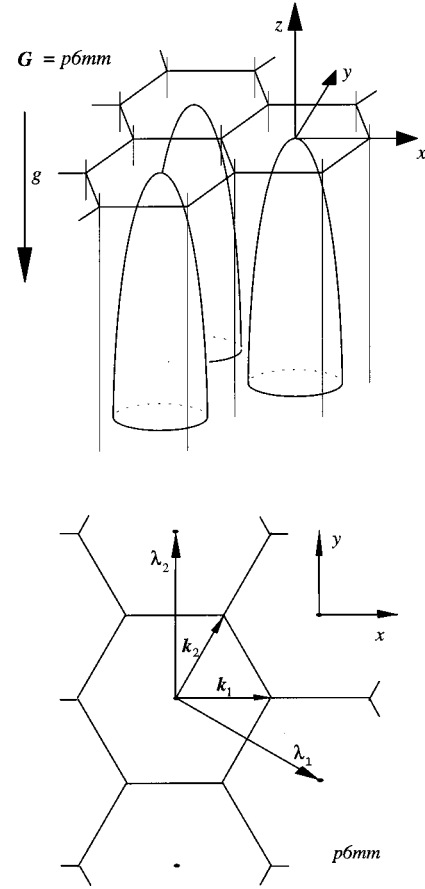
FIG. 2. Spatially periodic flow with invariance group $p6mm$. ''Air'' is coming up in the bubbles, ''water'' is coming down in the jets. Spatial periods λ_i and vectors of the inverse lattice $\mathbf{k}_i$. Black circles mark the positions of the bubble top.

the spatial flow. For a flow with high symmetry, $G=p6mm$ or $p4mm$, there is a one-parameter family of steady solutions with various values of the Froude number $F=\nu/\sqrt{g\lambda}$, whereas for the flow with group $G=pmm2$, the physical parameters of the problem (1) are $\{\nu,g,\boldsymbol{\lambda}_1,\boldsymbol{\lambda}_2 \neq G(\boldsymbol{\lambda}_1)\}$ and the steady solutions form a two-parameter family. At fixed values of acceleration and translations each solution of the multitude is an exact theoretical solution associated one-to-one with a free boundary, and with the form of the free boundary determined by the flow symmetry [18].

III. FAMILY OF STEADY SOLUTIONS

In this part of the paper we find the family of steady solutions for the flow with hexagonal symmetry group $p6mm$ and compare the results for various symmetries [6,7,13]. The approach we use for the free-boundary problem (1) is an asymptotic expansion, and it is detailed in the 3D case for symmetries $p4mm$ and $pmm2$ in [12,13].

For the invariance group $p6mm$, we find the analytical steady solutions by expanding the periodic potential and the free surface (1) in terms of the Laplace eigenfunctions. Let us switch to the frame of references moving upward with the steady velocity ν. Then,

$$\Phi(\mathbf{r},z) = \sum_{m=0}^{\infty} \Phi_m \left(3z + \frac{\exp(-mkz)}{mk} \sum_{i=1}^{3} \cos(m\mathbf{k}_i\mathbf{r}) \right)$$

$$+ (\text{cross terms}),$$

$$z^*(\mathbf{r}) = \sum_{m=0}^{\infty} z_m \sum_{i=1}^{3} \cos(m\mathbf{k}_i\mathbf{r}) + (\text{cross terms}). \tag{2}$$

Here $\mathbf{k}_{1,2}$ are the vectors of the inverse lattice, $\mathbf{k}_3 = \mathbf{k}_1 - \mathbf{k}_2$, with $k = |\mathbf{k}_i| = 4\pi/(\lambda\sqrt{3})$, $\mathbf{r} = (x,y)$, Fig. 2. $\{\Phi\}$ is the Fourier amplitude matrix. The steady flow (1) is smooth, so there are the relations

$$|\Phi_{m+1}| \ll |\Phi_m| \quad \text{and} \quad |z_{m+1}| \ll |z_m|. \tag{3}$$

In the unit cell, near the bubble top, the free boundary has the form

$$z^*(\mathbf{r}) = \sum_{n} \zeta_n \sum_{i=1}^{3} (\mathbf{k}_i\mathbf{r}/k)^{2n} + (\text{cross terms}). \tag{4}$$

The steady solutions (1) and (3) are analytical and

$$|\zeta_{n+1}| \ll |\zeta_n|. \tag{4'}$$

The free-boundary problem (1) can be formulated in terms of correlation functions or moments $\mathbf{M}$ generated by the Fourier amplitudes [9,13]. At $\mathbf{r} \approx 0, z \approx 0$ the equations at the free boundary take the forms $\Sigma_{i,j} D_{ij}(\mathbf{M},\zeta) x^{2i} y^{2j} = 0$ and $\Sigma_{i,j} U_{ij}(\mathbf{M},\zeta) x^{2i} y^{2j} = 0$, $i+j=N$, with "diagonal" moments $M_n = \Sigma_{m=1}^{\infty} \Phi_m(km)^n + (\text{cross terms})$ and velocity $\nu = -3M_0$. One obtains

$$\mathbf{r}^2(\zeta_1 + 3M_1^2/4)C_1 + \mathbf{r}^4(g\zeta_2 + 9\zeta_1^2 M_1^2 + M_2^2/4 - M_1 M_3/4)C_2$$

$$+ \cdots = 0, \tag{5}$$

$$\mathbf{r}^2(-6\zeta_1 M_1 - M_2/2)C_1 + \mathbf{r}^4(-9\zeta_2 M_1 + 9\zeta_1^2 M_2 + 3\zeta_1 M_3/2$$

$$+ M_4/4!)C_2 + \cdots = 0$$

for the Euler equation and for the kinematic equation (1), respectively ($C_1 = 3/2$, $C_2 = 9/8$).

We find N successive approximations of solutions (1) and (5) from self-consistent conditions for surface variables $\{\zeta\}$, and at each N we solve a chain of equations in variables $\mathbf{M}$. Symmetry separates among all correlators $\mathbf{M}$ the linearly independent ones. Some additional relationships between the correlators can be established at any finite N because of the flow properties (3) and (4').
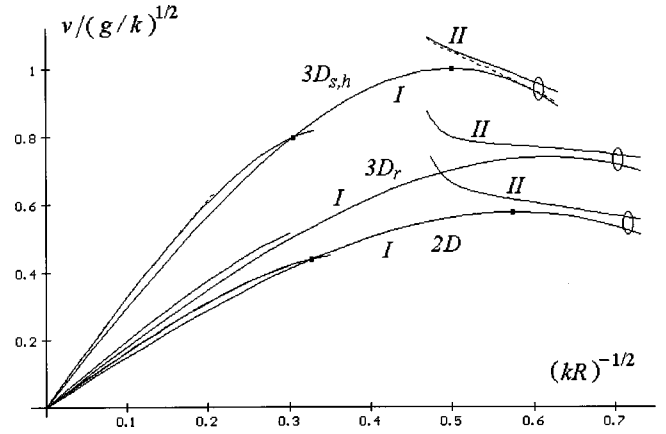
FIG. 3. Dependence of the velocity ν on parameter kR. Hexagonal $3D_h$ ($p6mm$), rectangular $3D_r$ ($pmm2$ [13]), square $3D_s$ ($p4mm$ [12]), and plane 2D ($pm11$ [9]) types of flow symmetry. Roman numerals denote the order of approximation. Dashed line marks the second-order solutions for $3D_s$ flow. For $3D_r$ flow just one of the cross sections of the two-parameter surface is shown: $k_y = k_x/2$ and $R_x/R_y = 0.04(k_y/k_x)^2$ with $k_x = k, R_x = R$. Black squares are "zero-parameter" solutions, circles mark edge solutions kR_{cr}.

At $N=1$, $M_n = \Sigma_{m=1}^{2} \Phi_m(km)^n$, the velocity $\nu = -3(\Phi_1 + \Phi_2) = (-9M_1 k + 3M_2)/2k^2$ and the curvature radius at the top of the bubble $R = -1/(3\zeta_1) = 4M_1/M_2 = 4g/9M_1^2$:

$$\nu = \sqrt{g/k}(3kR-4)/(kR)^{3/2}, \quad z^* = -(x^2+y^2)/2R,$$

$$\Phi_1 = -4\sqrt{g/k}(kR-2)/3(kR)^{3/2}, \tag{6}$$

$$\Phi_2 = \sqrt{g/k}(kR-4)/3(kR)^{3/2}.$$

At $R = 12/(5k)$ in Eqs. (6), $\Phi_2 = \Phi_1$, and the conditions (3) and (4') break. So the physical region of the parameter values in Eqs. (6) is defined as $12/(5k) < R < \infty$. Maximal velocity in Eqs. (6), $\nu = \sqrt{g/k}$, peaks at $R = 4/k$ for the "zero-parameter" solution with $\Phi_2 = 0$, Fig. 3. Note that at $N=1$, "hexagonal" and "square" flows remain axisymmetric, $z^* \sim (x^2+y^2)$, and the expressions (6) and [12] for the velocity and the free surface coincide within the normalized factor k, Fig. 3. Moreover, the renormalized "maximal" solution reproduces Layzer's result [6] (to show this, one needs to expand in Taylor's consideration [4] the flow potential and the stream function in the lowest order of z and r).

In spite of the above agreement, the real behavior of steady solutions (1) is more complex. At $N=2$ in Eqs. (2)–(4), $M_n = \Sigma_{m=1}^{3} \Phi_m(km)^n$, the velocity $\nu = -3(\Phi_1 + \Phi_2 + \Phi_3)$, and one finds

$$\nu = 2\sqrt{g/k}[15(kR)^3 - 124(kR)^2 + 216kR - 144]/9(kR)^{5/2}(kR-6),$$

$$\tag{7}$$

$$z^* = -(x^2+y^2)/2R - (x^2+y^2)^2[3(kR)^3 - 22(kR)^2 + 60kR - 72]/24R^3(kR-6).$$
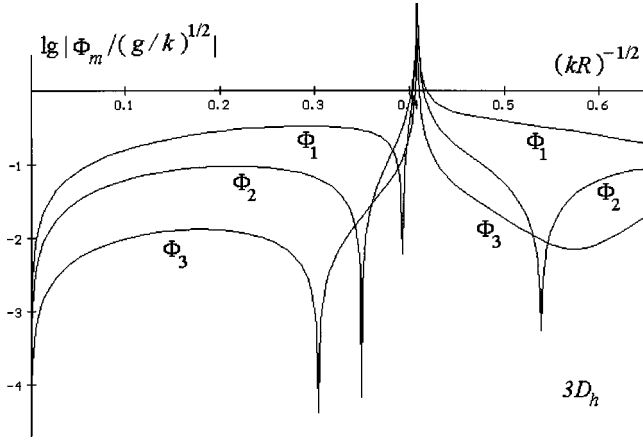
FIG. 4. Family of steady solutions in RTI for "hexagonal" flow $3D_h$, $N=2$. Decreasing of Φ_m with an increase in m in the physical region of the parameter.

FIG. 5. The family of steady solutions in the "narrow-bubbles" region for hexagonal $3D_h$ ($p6mm$), square $3D_s$ ($p4mm$ [12]), and plane 2D ($pm11$ [9]) types of flow symmetry. λ is the spatial period. Roman numerals denote the order of approximation. Black squares are renormalized Layzer's solutions, $R=4/k$, $\nu=\sqrt{g/k}$ in 3D ($3D_t$ tubular flow) and $R=3/k, \nu=\sqrt{g/3k}$ in 2D.

The solution with $\Phi_3=0$ in Eqs. (7) corresponds to $R = 10.843/k$ and $\nu = 0.799\sqrt{g/k}$. These values are far from the "maximal" solution in Eqs. (6) with $R=4/k$ and $\nu=\sqrt{g/k}$, so "zero-parameter" solutions (1) diverge with an increase in N, Fig. 3. Alternatively, in the physical region, there is a functional convergence of approximated solutions over the parameter R, Figs. 3 and 4. In accordance with Eqs. (3) and (4′), we evaluate for $\forall N$ ($V>0$, Fig. 4)

$$\left| [\nu(R)]_{N+1} - [\nu(R)]_N \right| \approx V \times 10^{-N},$$

$$\left| \Phi_m(R)/\Phi_1(R) \right| \approx 10^{-m}. \tag{8}$$

The difference between the one-parameter solutions (6) and (7) in the region of narrow bubbles is minimal at $R = 3.032/k$ and $\nu = 0.987\sqrt{g/k}$ with $\Phi_2/\Phi_1 = 0.14$, while at $R<3.032/k$ the convergence becomes worse and at $R = 2.4/k$ ($\nu = 0.916\sqrt{g/k}$) the relation $\Phi_2/\Phi_1 = 0.44$. In higher approximations, the function of velocity slightly exceeds solution (6), Fig. 3.

The analysis of the obtained results is as follows. The physical region of parameter values is $kR_{cr} \leqslant kR \leqslant \infty$. The velocity dependence over the family of solutions is nonmonotone. Similarly to [9,12,13], the first approximation is the best and smooth for kR in the interval $kR_{cr} \leqslant kR \leqslant \infty$, Fig. 3. Over a wide range of parameters the difference between the approximated curves of solutions (6) and (7) (velocity or each of the Fourier amplitudes) is exponentially small. For each given approximation the absolute values of the Fourier amplitudes Φ_m decrease with increasing amplitude number m, Eqs. (8), Fig. 4. In this way, the existence of a unique one-parameter family of steady solution is indicated as a functional limit over the parameter R, Figs. 3 and 4.

"Narrow bubbles" with $kR_{cr} \leqslant kR \leqslant kR_{max}$, "medium bubbles" with $kR_{max} < kR < \infty$, and "solitary jets" with $kR \to \infty$ can be separated in the physical region of parameter values, Fig. 3. The region of "narrow bubbles" is bounded by values kR_{cr} and $\sim kR_{max}$. The critical curvature radius, kR_{cr}, is the edge of the physical solutions. At $kR \approx kR_{cr}$ for any N, the conditions (3) and (4′) are broken, Figs. 3 and 4,

and the approximations diverge: bubbles cannot be too narrow. We roughly estimate $R_{cr} = (2.716 \pm 0.316)/k$ with $\nu_{cr} = (0.955 \pm 0.035)\sqrt{g/k}$. Expressions (6) and (7) allow us to evaluate the "maximum solution" as $\nu_{max} \approx 1.05\sqrt{g/k}$ with $kR_{max} \approx 4$, Fig. 3 [$kR = 3.917$ is the inflection point for velocity (7)]. At $kR_{cr} \leqslant kR \leqslant kR_{max}$, $R \sim (\lambda/2)$, successive approximations converge well exponentially, Eqs. (8), Figs. 3 and 4. Interestingly, as the bubble radius increases, at $kR > kR_{max}$, the convergence becomes worse. For these "medium bubbles" with $kR_{max} < kR < \infty$ and $R \geqslant (\lambda/2)$, jet motion is important and the asymptotic expansions (2) and (4) cannot describe the flow correctly, Figs. 3 and 4. We evaluate the poorly approximated region of "medium" bubbles as $4.7 < kR < 9.2$ [the velocity $\nu > 1.1\sqrt{g/k}$ at $4.611 < kR < 6$ in Eqs. (7)], Fig. 3. Nevertheless, for very large values of curvature radius, $kR \to \infty$ and $R/(\lambda/2) \to \infty$, the free boundary problem (1) can be considered as a problem of jets passing through periodic holes (slots) in the plane (x,y) [19]. For these "solitary jets," conditions (3) and (4′) are met, and approximations converge, Figs. 3 and 4. When $kR \to \infty$, Fourier amplitudes $\Phi \approx 1/\sqrt{kR}$, the velocity is expected as $\nu \to 4\sqrt{g/(k^2R)}$ with $F \to 0$ [Eqs. (6) and (7) [13]].

Let us compare the basic features of the results obtained in the symmetries $p6mm$ [Eqs. (6) and (7)], $p4mm$ [12], $pmm2$ [13], and $pm11$ [9,13], Figs. 3 and 5. These results share a number of common properties. The equations in moments and the solutions are very similar; narrow bubbles and solitary jets are typical regions of steady families, Figs. 3 and 5. When the flow is invariant with respect to these symmetry groups, there is a convergence of successive approximations as the functional limit over the parameter (or parameters for "rectangular" flow $pmm2$). Reducing that multitude dimension required by symmetry immediately leads one to a divergence of successive approximations and, in general, removes approximated solutions from the physical region [12,13]. The dependence of the approximated solutions on a specific

choice of truncations in the physical region is weak [12,13] [Eqs. (6) and (7)]. Methods (2) and (4) and [12,13] can be considered as a general approach to the problem of steady motion in RTI for all kinds of spatial symmetries.

To make a quantitative comparison of the results at different symmetries, we need to choose the appropriate length scale. In dimensionless units $\sqrt{g/k}$ and $1/k$, ''square'' and ''hexagonal'' one-parameter families of solutions are weakly differing, Fig. 3. Bubbles remain near axisymmetric for both symmetries, $z^* \sim (x^2 + y^2)/R$, and the ''dimensionless'' theoretical description is a universal one for these one-parameter families of steady solutions. Remember that the value of the wave vector **k** depends significantly on the lattice, Eqs. (2) [20]. At fixed wavelength λ, 3D hexagonal flow is slower than 3D square flow [12,13], whereas hexagonal bubbles are narrower than square ones, Fig. 5, and, naturally, 3D flow is faster than 2D flow [2,5,6].

Note that wavelength λ of the initial perturbation (or tube diameter for tubular flow) is a parameter that can be easily controlled experimentally [3,4]. The bubble radius R is the free parameter of the steady solutions family in problem (1). At a fixed value of translation λ, the radius of the steady bubble is subject to wide variations, from $\sim \lambda/2$ to infinity, Fig. 3. So the wavelength λ, not the bubble radius, is the basic length scale in problem (1). The bubble velocity and the bubble radius of curvature are the quantities to be measured in the Rayleigh-Taylor instability.

To separate a unique significant flow in the family of steady solutions (1), the linear stability analysis has been performed in [20] recently. The results show us that for hexagonal flow $p6mm$ [Eqs. (6) and (7)] (and, thus, for square flow $p4mm$ [12]), the ''maximal solution'' with $\nu_{max} \approx 1.05 \sqrt{g/k}$ and $kR_{max} \approx 4$ is stable, whereas solitary jets and medium bubbles are unstable.

As far as we know, no experiments have been carried out to study quantitatively the effect of flow spatial symmetry on the RT instability, and, unfortunately, there are no sufficient experimental data on the bubble radius [4,5,10,11,16]. For 3D steady flow, Taylor's result [4] in a tube is $\nu = 0.49 \sqrt{g(\lambda/2)}$; Read's measurements for 3D periodic motion [5] give a larger value, $\nu = 0.51 \sqrt{g(\lambda/2)}$. The numerical simulations performed by Li for ''square'' compressible flow with Atwood number about unity [11] give values $\nu/\sqrt{g(\lambda/2)} = 0.57 - 0.59$. Although ''experimental'' bubbles are slower than ''theoretical'' ones, these values of velocity agree with our solutions. It should be noted that Taylor's velocity $\nu = 0.49 \sqrt{g(\lambda/2)}$ [4] is close to the ''hexagonal'' one-parameter family of steady solutions (and maximum so-

lutions $p6mm$), rather than the ''square'' one, and the value [4] can never be obtained for a flow with square symmetry $p4mm$, Fig. 5 [12]. Clearly, the hexagonal lattice is the closest to the flow with ''cylindrical'' properties, and the hexagonal symmetry of problem (1) gives one more adequate description of Taylor's experiment.

IV. CONCLUSION

It this paper we shown the following.

There is an experimental region, where the Rayleigh-Taylor instability can be studied on the basis of symmetry theory. The symmetry approach allows us to analyze the stability of steady periodic structures with respect to disruptions of the macroscopic homogeneity. The steady motion can be generated by RTI, if initial perturbation is invariant with respect to symmorphic groups posing inversion, such as hexagonal, square, rectangular, oblique, or rhombic groups. Notice that this condition is necessary but not sufficient. Starting from this condition, the local stability analysis [20] poses harder requirements (no splitting instabilities), and now it seems likely that periodic steady motion in RTI can be observed for high-symmetric groups $p6mm$ and $p4mm$ only.

The asymptotic expansion at the bubble top in terms of moments is a general approach to the steady problem (1) in RTI. The method gives one the family of steady solutions for 3D [Eqs. (6) and (7) [12,13]] and 2D flows, and the number of the family parameters is determined by the flow symmetry. Results obtained for various symmetries share a number of common properties. For high-symmetric flows, the families of steady solutions get a universal theoretical description in dimensionless units.

For 3D flows there are no sufficient experimental data, and measurements of the steady bubble velocity and its radius of curvature allow one to evaluate the correctness of the theory.

As was already noted, in real fluids the ''experimental'' bubbles are slower than the theoretical ones. Studying of jet motion (boundary layer for a flow in a tube) for compressible and viscous fluids would eliminate this discrepancy.

[1] Lord Rayleigh, in *Investigations of the Character of the Equilibrium of an Incompressible Heavy Fluid of Variable Density*, special issue of Proc. London Math. Soc. **14**, 170 (1883).

[2] D. H. Sharp, Physica D **12**, 3 (1984).

[3] S. Chandrasekhar, *Hydrodynamic and Hydromagnetic Stability* (Oxford University Press, Oxford, 1961); K. O. Mikaelian, Phys. Rev. E **47**, 375 (1993).

[4] R. M. Davies and G. I. Taylor, Proc. R. Soc. London, Ser. A **200**, 375 (1950).

[5] K. I. Read, Physica D **12**, 45 (1984).

[6] D. Layzer, Astrophys. J. **122**, 1 (1955).

[7] P. R. Garabedian, Proc. R. Soc. London, Ser. A **241**, 423 (1957).

[8] G. Birkhoff and D. Carter, J. Math. Mech. **6**, 769 (1957).

[9] N. A. Inogamov, Pis'ma Zh. Eksp. Teor. Fiz. **55**, 505 (1992) [JETP Lett. **55**, 521 (1992)].

[10] D. L. Youngs, Phys. Fluids A **3**, 1312 (1991); P. F. Linden, J. M. Redondo, and D. L. Youngs, J. Fluid Mech. **265**, 97 (1994).

[11] X. L. Li, Phys. Fluids A **5**, 1904 (1993); Phys. Fluids **8**, 336 (1996).

[12] S. I. Abarzhi and N. A. Inogamov, Zh. Eksp. Teor. Fiz. **107**, 245 (1995) [JETP **80**, 132 (1995)].

[13] S. I. Abarzhi, Zh. Eksp. Teor. Fiz. **110**, 1841 (1996) [JETP **83**, 1012 (1996)]; Phys. Scr. **T66**, 238 (1996).

[14] A. V. Shubnikov and V. A. Koptsik, *Symmetry in Science and Art* (Plenum, New York, 1979).

[15] L. Landau and E. Lifshitz, *Statistical Physics* (Addison-Wesley, Reading, MA, 1959).

[16] F. H. Harlow and J. E. Welch, Phys. Fluids **9**, 842 (1966); R. Menikoff and C. Zemach, J. Comput. Phys. **51**, 28 (1983); G. R. Baker, D. I. Meiron, and S. A. Orszag, Phys. Fluids **23**, 1485 (1980); B. A. Remington *et al.*, Phys. Rev. Lett. **73**, 545 (1994).

[17] G. Hazak, Phys. Rev. Lett. **76**, 4167 (1996).

[18] D. Youngs, Physica D **12**, 32 (1984); Physica D **37**, 270 (1989).

[19] L. Landau and E. Lifshitz, *Fluid Mechanics*, 2nd ed. (Pergamon, Oxford, 1987).

[20] S. I. Abarzhi, Phys. Rev. Lett. **89**, 1332 (1998).